

Discrimination of Composite Graphite Samples Using Remote Filament-Induced Breakdown Spectroscopy

Elizabeth J. Judge, George Heck, Elizabeth B. Cerkez, and Robert J. Levis*

Temple University Department of Chemistry, 1901 North 13th Street, Philadelphia, Pennsylvania 19122

Remote filament-induced breakdown spectroscopy (R-FIBS) using ultrashort laser pulses was used to measure the carbon/clay ratios between three graphite composites of different hardness at a standoff distance of ~6 m. Measurements using R-FIBS and femtosecond laser-induced breakdown (fs-LIBS) reveal similar selectivity and ability to excite emission. Comparison of the two standoff techniques with optical microscopy and electron microprobe point detection confirmed the qualitative analysis capability of both femtosecond remote probing techniques. The R-FIBS technique produced more accurate results compared to fs-LIBS due to the intensity clamping nature of the filament ablation source. Measurement of the plasma temperatures for the metallic emission lines (~8500 K) and the C₂ Swan lines (~4500 K) suggest that the plasmas from different microdomains (clay and graphite) are not in equilibrium.

Laser induced breakdown spectroscopy (LIBS) is an established atomic emission spectroscopy technique that uses high-energy laser pulses for excitation of solid targets. LIBS has been used to determine the elemental composition of a variety of materials including works of art,¹ clay artifacts,² soils,^{3,4} trees,⁴ metals,⁵ glass,⁶ biological materials,^{7,8} explosive material,⁹ and gases.¹⁰ LIBS technology has been reviewed.¹¹ Standoff fs-LIBS has also been used to detect copper with a detection limit of 100

ng at 25 m.¹² Remote filament-induced breakdown spectroscopy (R-FIBS) is a more recent technique that utilizes the intense core of a filament (~10¹³ W/cm²) formed in a femtosecond laser pulse propagating through the atmosphere.¹³ R-FIBS is an attractive analytic tool because it requires no sample preparation, provides virtually instantaneous identification of elements, and is a technology providing facile remote detection capability because no focusing optics are required to induce plasma formation.

In the LIBS technique, a microsecond to femtosecond laser pulse is focused onto a target causing ablation of the material. A plasma is formed above the surface of the material consisting of excited ions, atoms, and molecules. Temperatures ranging from 3 000 to 20 000 K can occur, depending on laser parameters including intensity, pulse duration, and central frequency. As the plasma plume expands at supersonic speeds, emission of light occurs via atomic transitions from higher to lower electronic energy states, allowing identification of the material from the resulting emission spectrum. The plasma not only has atomic and molecular emission, which produces spectrally sharp peaks due to electronic transitions but it also displays continuum emission. The continuum is a result of two processes: recombination of electrons with ions and Bremsstrahlung emission, which together produce a spectrally broad signal.

Since the introduction of remote filament-induced breakdown spectroscopy, (R-FIBS) the method has been used successfully to detect atomic emission lines from copper and steel at a distance of 180 m from the laser system¹⁴ and biological materials at distance of 3 m.⁷ Here, we describe the first investigation of complex composite materials using a high-resolution spectrometer to resolve atomic lines. In R-FIBS, the airborne filament resulting from self-focusing of an intense femtosecond laser beam is used as the excitation source to create a plasma. Conversely, in LIBS, the plasma is generated by focusing the laser beam using a lens (geometric focusing). Filaments achieve intensities reaching 4 ×

* To whom correspondence should be addressed. E-mail: rjlevis@temple.edu.

- (1) Detalle, V.; Glorieux, Q.; Bruder, R.; L'Hermite, D.; Semerok, A. *Actual. Chim.* **2007**, *312*, 98–104.
- (2) Tzortzakis, S.; Anglos, D.; Gray, D. *Opt. Lett.* **2006**, *31*, 1139–1141.
- (3) Lazic, V.; Rauschenbach, T.; Jovicevic, S.; Jessberger, E. K.; Fantoni, R.; Di Fino, M. *Spectrochim. Acta, Part B: At. Spectrosc.* **2007**, *62*, 1546–1556.
- (4) Lopez-Moreno, C.; Palanco, S.; Laserna, J. J. *J. Anal. At. Spectrom.* **2004**, *19*, 1479–1484.
- (5) Liu, W.; Xu, H. L.; Mejean, G.; Kamali, Y.; Daigle, J. F.; Azarm, A.; Simard, P. T.; Mathieu, P.; Roy, G.; Chin, S. L. *Spectrochim. Acta, Part B: At. Spectrosc.* **2007**, *62*, 76–81.
- (6) Carmona, N.; Oujja, M.; Gaspard, S.; Garcia-Heras, M.; Villegas, M. A.; Castillejo, M. *Spectrochim. Acta, Part B: At. Spectrosc.* **2007**, *62*, 94–100.
- (7) Xu, H. L.; Liu, W.; Chin, S. L. *Opt. Lett.* **2006**, *31*, 1540–1542.
- (8) Xu, H. L.; Mejean, G.; Liu, W.; Kamali, Y.; Daigle, J. F.; Azarm, A.; Simard, P. T.; Mathieu, P.; Roy, G.; Simard, J. R.; Chin, S. L. *Appl. Phys. B: Lasers Opt.* **2007**, *87*, 151–156.
- (9) Lopez-Moreno, C.; Palanco, S.; Laserna, J. J.; DeLucia, F.; Miziolek, A. W.; Rose, J.; Walters, R. A.; Whitehouse, A. I. *J. Anal. At. Spectrom.* **2006**, *21*, 55–60.
- (10) Xu, H. L.; Kamali, Y.; Marceau, C.; Simard, P. T.; Liu, W.; Bernhardt, J.; Mejean, G.; Mathieu, P.; Roy, G.; Simard, J. R.; Chin, S. L. *Appl. Phys. Lett.* **2007**, *90*, 101106.

- (11) Radziemski, L. J. *Spectrochim. Acta, Part B: At. Spectrosc.* **2002**, *57*, 1109–1113.
- (12) Rohwetter, P.; Yu, J.; Mejean, G.; Stelmaszczyk, K.; Salmon, E.; Kasparian, J.; Wole, J. P.; Woste, L. *J. Anal. At. Spectrom.* **2004**, *19*, 437–444.
- (13) Stelmaszczyk, K.; Rohwetter, P.; Mejean, G.; Yu, J.; Salmon, E.; Kasparian, J.; Ackermann, R.; Wolf, J. P.; Woste, L. *Appl. Phys. Lett.* **2004**, *85*, 3977–3979.
- (14) Rohwetter, P.; Stelmaszczyk, K.; Woste, L.; Ackermann, R.; Mejean, G.; Salmon, E.; Kasparian, J.; Yu, J.; Wolf, J. P. *Spectrochim. Acta, Part B: At. Spectrosc.* **2005**, *60*, 1025–1033.

10^{13} W/cm² through self-focusing in air,¹⁵ which is well above the intensity threshold for ablation in all materials. This is above the threshold (typically $\sim 10^9$ W/cm² but depends on laser and sample properties) for stoichiometric ablation of a solid,¹⁶ suggesting that filaments should induce an emission signal that is representative of the elemental ratios found in the material.

The phenomena of filamentation has been recently reviewed.^{17,18} In general, if a laser beam has a power exceeding the critical value for filamentation, Kerr lensing dominates diffraction effects and the beam will self-focus to high intensities. However, the beam will not continue to self-focus indefinitely. This is due to an effect called intensity clamping.¹⁹ In air, when the beam reaches 10^{13} W/cm², ionized electrons are generated. Free electrons create a negative lens effect on the pulse.¹⁷ When the density of free electrons reaches $\sim 5 \times 10^{14}$ cm⁻³, the negative lens counterbalances the self-focusing of the pulse, resulting in intensity clamping. The intensity of the pulse which generates this free electron density is 5×10^{13} W/cm² in air. The length of the region where plasma defocusing and Kerr focusing are in a stable equilibrium can be continuous for several hundred meters.^{20,21} In addition to geometrical changes to the femtosecond laser pulse during filamentation, there are spectral changes as well. The spectrum of an 800 nm laser beam, which has achieved filamentation, will contain a broad continuum of light that can extend from 250 nm to the terahertz region.¹⁷

In nanosecond LIBS, the standoff distance is related to the numerical aperture of the optics (limited by the diameter of the focusing optic) and the available laser energy.²² In the case of R-FIBS, no focusing optics are necessary, and the filament can propagate over long distances with constant power.¹⁴ Two interesting properties of filament-based remote probing are the intensity clamping in the filament and the unique capability to control the length and position in space by shaping the spectral phase of the pulse at the laser source.²³ Calculations have shown that R-FIBS could be effective up to a kilometer in distance,¹³ which makes R-FIBS an exciting new technique with many possible applications such as remote detection of biological materials and atmospheric pollution.

Femtosecond pulses have lower ablation fluence thresholds in comparison to nanosecond pulses.²⁴ At the same fluence as a nanosecond pulse, a femtosecond pulse produces lower continuum emission, ablates roughly the same amount of material (in Cu this is 2000 $\mu\text{m}^3/\text{mJ}$), and produces lower spectral line intensi-

ties when integrated over the plasma lifetime in comparison to nanosecond pulses.^{24,25} In the case of nanosecond pulses, the plasma formed in the first few picoseconds will subsequently interact with the remainder of the pulse. The longer interaction time between the nanosecond laser and the developing plasma causes melting and vaporization of the sample and ionization via electron-ion collisions.²⁶ This in turn causes higher atomic emission but also higher background continuum emission. The lower continuum emission in femtosecond laser excitation allows nongated detection to be used.²⁷

In this paper we compare fs-LIBS and R-FIBS of complex composite materials using high-resolution optical spectroscopy for the first time. The complex composite materials are a series of carbon targets doped with varying degrees of metal oxides obtained from commercial pencil cores. We investigated the C₂/Al and C₂/K emission ratios for these composites to discriminate between samples that are very similar in composition. The ability of a standoff technique to accurately discriminate between similar samples is imperative for the technique to be used with confidence. These results are compared to electron microprobe measurements from the same samples. The plasma temperature for R-FIBS and fs-LIBS were also calculated in two ways: (1) from Boltzmann plots of C₂ Swan system emission lines and (2) from the ratios of aluminum/potassium emission lines.

EXPERIMENTAL SECTION

The experimental setup for fs-LIBS and R-FIBS is shown in Figure 1. A Ti:sapphire laser system, operating at 500 Hz, 800 nm central wavelength, 3 mJ per pulse with 60 fs pulse duration, was used to ablate the samples. The target samples for these experiments were Dixon Ticonderoga pencils, numbers 2, 2.5, and 3. These samples were chosen to investigate the discrimination power of fs-LIBS and R-FIBS for similar condensed phase solid samples. The targets were mounted on a translation stage that moved at a rate of 0.75 mm/s to provide new sample for interrogation. The 500 Hz repetition rate and 520 μm focused beam spot size resulted in 330 laser shots per sample spot, which removed approximately 130 μg of material per shot.

To perform the fs-LIBS experiment, the sample was placed 5.2 m from the 5.8 m focal length lens as seen in Figure 1. A plasma was formed on the sample and induced emission from the targets. The backscatter from the emission was collected with a 14 in. Meade LX 200R telescope with Ritchey-Chretien optics, at a distance of approximately 10 m from the target. The transmission coatings on the telescopes optics permit maximum transmission for spectral region from 450 to 750 nm and the transmission decreases significantly to 50% by 340 nm and near zero by 300 nm. All spectra were corrected for the transmission coatings effect. The light collected from the telescope was focused into a 50 μm i.d. fiber optic cable connected to an Andor Mechelle spectrometer with an iStar ICCD camera. The instrument was

(15) Braun, A.; Korn, G.; Liu, X.; Du, D.; Squier, J.; Mourou, G. *Opt. Lett.* **1995**, *20*, 73–75.

(16) Wing, T. C.; Russo, R. E. *Spectrochim. Acta, Part B: At. Spectrosc.* **1991**, *46*, 1471–1486.

(17) Couairon, A.; Mysyrowicz, A. *Phys. Rep.: Rev. Sect. Phys. Lett.* **2007**, *441*, 47–189.

(18) Chin, S. L.; Brodeur, A.; Petit, S.; Kosareva, O. G.; Kandidov, V. P. *J. Nonlinear Opt. Phys. Mater.* **1999**, *8*, 121–46.

(19) Kasparian, J.; Sauerbrey, R.; Chin, S. L. *Appl. Phys. B: Laser Opt.* **2000**, *71*, 877–879.

(20) La Fontaine, B.; Vidal, F.; Jiang, Z.; Chien, C. Y.; Comtois, D.; Desparois, A.; Johnston, T. W.; Kieffer, J. C.; Pepin, H.; Mercure, H. P. *Phys. Plasmas* **1999**, *6*, 1615–1621.

(21) Champeaux, S.; Berge, L. *Phys. Rev. E: Stat., Nonlinear, Soft Matter Phys.* **2003**, *68*, 066603.

(22) Hecht, E. *Optics*, 4th ed; Pearson Education, Inc.: San Francisco, CA, 2002; p 195, p 215.

(23) Heck, G.; Sloss, J.; Levis, R. J. *Opt. Commun.* **2006**, *259*, 216–222.

(24) Semerok, A.; Salle, B.; Wagner, J. F.; Petite, G. *Laser Part. Beams* **2002**, *60*, 67–72.

(25) Sirven, J. B.; Bcusquet, B.; Canioni, L.; Sarger, L. *Spectrochim. Acta, Part B* **2004**, *103*, 3–1039.

(26) Eland, K. L.; Stratis, D. N.; Gold, D. M.; Goode, S. R.; Angel, S. M. *Appl. Spectrosc.* **2001**, *55*, 286–291.

(27) Miziolek, A. W.; Palleschi, V.; Schechter, I., Eds.; *Laser-Induced Breakdown Spectroscopy (LIBS): Fundamentals and Applications*; Cambridge University Press: Cambridge, U.K., 2006; p 620.

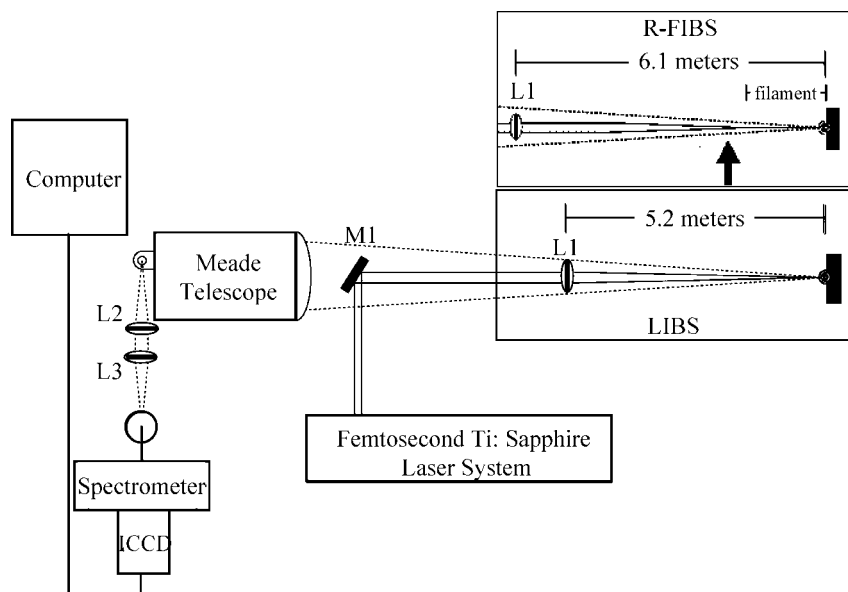


Figure 1. fs-LIBS and R-FIBS experimental setup for remote detection of pencils. M1, 45° dielectric coated mirror; L1, 5 m focusing lens; L2 and L3, collimating and focusing lenses into spectrometer. The arrow in the R-FIBS setup shows the beginning of the filament.

calibrated for wavelength and intensity response using a D_2 and tungsten source. Gating was used to eliminate the reflected laser emission at 800 nm. A delay of 120 ns, gain of 200, and gate width of 1 μ s was used to acquire the signal. In the second experiment, R-FIBS, the sample was placed 6.1 m behind the 5.8 m lens. This allowed for filament formation at 5.4 m from the lens, and this filament was used to ablate the target, see Figure 1. The broadband signal of the filament was gated out by using the same delay conditions. All other parameters were the same as the LIBS experiment. The intensity profile of the beam was imaged on Kodak burn paper to confirm that a filament formed. First, a chirped 1 ps pulse was imaged using the burn paper, and the diameter at the 5.2 m focus was 0.8 mm and the diameter 10 m from the lens was 3.6 mm. In contrast, the diameter of the 60 fs pulse used in the R-FIBS experiment was 0.85 mm, 6 m from the lens, increasing to 1.2 mm, 10 m from the lens. The small increase in the filament's diameter over 4 m is evidence of filament formation with propagation over several meters.

The carbon composites used in this investigation were obtained from commercially available Ticonderoga pencils numbers 2, 2.5, and 3. We chose these composite materials because pencils of different hardness vary in graphite and clay composition by reproducible amounts and are complex materials. The amount of graphite in the pencil samples was determined with a Nikon Eclipse E600 POL optical microscope. Sample image areas of $160 \times 200 \mu\text{m}$ with 40 \times magnification were used to determine the percent graphite with software (ImageJ), which compares the fraction of the surface that reflects light (graphite) and absorbs light (clay). A JEOL 733 electron microprobe was used in this experiment to provide independent measurement of atomic concentrations. The graphite core was first submerged in epoxy and heated at 175 °C for 1½ h. The samples were then polished flat using seven different grits ranging from 300 to 1 μm . The samples were analyzed using a 15 keV electron microprobe. X-rays are emitted from the sample, through the Auger processes, and detected with a lithium drifted silicon (Si(Li)) energy dispersive detector (EDS). A sample area of 275×375

μm^2 was probed for three different areas on a single pencil to acquire an averaged spectrum.

Safety Considerations. Several safety precautions were taken since the laser was directed off of the laser table to perform the measurements. Appropriate laser eye protection was worn by all personnel. The area of the laboratory where the laser propagated was sectioned off to prevent accidental exposure to the laser beam.

RESULTS AND DISCUSSION

Remote Filament Induced Breakdown Spectroscopy. The atomic emission spectra of the pencils were collected in a stand-off configuration using both the fs-LIBS and R-FIBS excitation modes. Figure 2a,b compares the emission spectra from a plasma produced on a no. 2 pencil ablated in the fs-LIBS and R-FIBS configurations. A series of emission features are observed in both excitation experiments. The emission lines associated with graphite are the C_2 Swan system of carbon emission bands ($d^3 \Pi_g - a^3 \Pi_u$) at 467–473, 507–516, and 544–563 nm and the CN Violet system ($B^2 \Sigma^+ - X^2 \Sigma^+$) at 385–391 nm. The emission from the CN molecular fragment has been attributed to the reaction between ablated C_2 fragments and atmospheric N_2 ($C_2 + N_2 \rightarrow 2CN$).⁸ The features corresponding to the clay component in the targets consist of Al I peaks at 394.4 nm ($3s^2 3p^2 P^\circ - 3s^2 4s^2 S$) and 396.15 nm ($3s^2 3p^2 P^\circ - 3s^2 4s^2 S$), and K I peaks at 766.49 nm ($3p^6 4s^2 S - 3p^6 4p^2 P^\circ$) and 769.89 nm ($3p^6 4s^2 S - 3p^6 4p^2 P^\circ$). The emission peaks at 422 and 670 nm are from calcium and lithium, respectively, and are known contaminants of clay. The spectral features were assigned using data from the NIST atomic spectra database.

To compare fs-LIBS and R-FIBS, several parameters must be considered including the laser intensity, plasma temperature, and ablation efficiency. The laser intensity interacting with the surface is a function of the focal spot size, pulse duration, and the energy in the beam. With the use of low power to minimize Kerr lensing, the measured focal length of the lens was 5.8 m. Kerr lensing in the intense laser beam shortens the focal length to 5.2 m for the fs-LIBS experiment. Thus, the target was placed 5.2 m from the

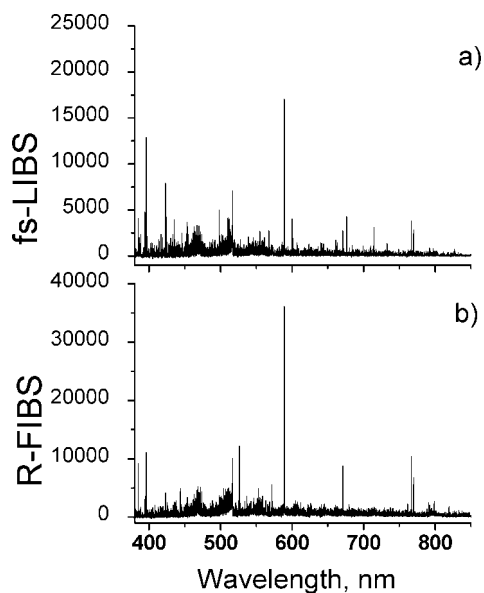


Figure 2. (a,b) Emission spectra from the graphite/clay core of no. 2 pencil for (a) fs-LIBS and (b) R-FIBS. The contaminant sodium at 588 nm dominates the spectra. Aluminum (364 and 396 nm), calcium (422 nm), C₂ Swan System (see text for emission lines), lithium (670 nm), and potassium (766 and 769 nm) emission lines can also be seen in both spectra.

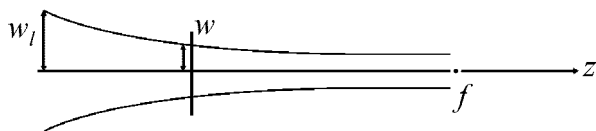


Figure 3. Illustration of the contraction of a Gaussian beam under geometrical and self-focusing conditions. The beam radius at the lens is w_L , the beam radius at a distance z from the lens is w_z , and the focal distance of the lens is f .

lens. Figure 3 illustrates the contraction of a Gaussian beam under geometrical and self-focusing conditions. The focused spot radius at the LIBS focal point (5.2 m), $w(z)$, can be calculated using eq 1, which takes into account both the Kerr lens and geometric focusing processes.

$$w^2(z) = w_L^2 \frac{\alpha f^2}{1 + \alpha f^2} \left(1 + \alpha \left(\frac{1 + \alpha f^2}{\alpha f^2} \right)^2 \left(\frac{f}{1 + \alpha f^2} - z \right)^2 \right) \quad (1)$$

$$\alpha = \frac{1}{k^2 w_L^4} \left(1 - \frac{P}{P_C} \right) \quad (2)$$

where z is the distance from the lens in which the beam waist is being calculated, f is the focal length of the lens, w_L is the radius of the collimated beam at the focusing lens, k is the wavenumber, P is the power of the beam, and P_C is the critical power, which is 3.2 GW in air at 800 nm.¹⁷ The calculated focal spot size, using eq 1, was 520 μm in diameter providing an intensity on the target of 2.3×10^{13} W/cm² for fs-LIBS. Kerr lensing¹⁷ and intensity clamping¹⁷ in R-FIBS creates an intensity of 5×10^{13} W/cm². The energy density of fs-LIBS and R-FIBS was 1.4 and 3.0 J/cm², respectively. Plasma temperature and ablation efficiency of both methods will be discussed in the following section.

Discriminating Similar Composition Samples: Atomic Ratio Analysis. Discrimination between the samples varying in graphite concentration was attempted by atomic ratio analysis from

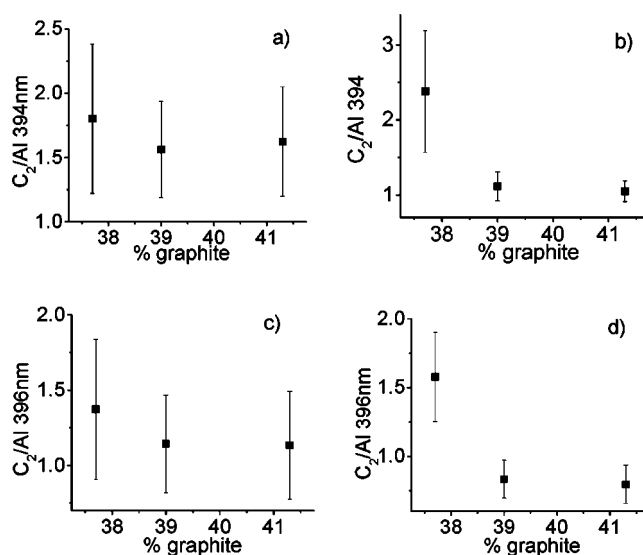


Figure 4. (a–d) A plot of C₂/Al 394 nm emission line intensity ratios as a function of percent graphite in the composite for (a) fs-LIBS and (b) R-FIBS. A plot of the C₂/Al 396 nm emission line intensity ratios as a function of percent graphite in the composite for (c) fs-LIBS and (d) R-FIBS.

the fs-LIBS and R-FIBS measurements. The spectra from three pencil types were used to determine the line intensity of the C₂ Swan line at 516.5 nm and the clay emission from Al I and K I peaks. The peak intensity was calculated by subtracting the baseline from the peak height. The peak intensities of the Al I lines and C₂ band at 516 nm were then used to determine the C₂ emission to clay element ratio. These ratios were determined for each pencil. Figure 4a–d shows C₂/Al 394 nm and C₂/Al 396 nm for both fs-LIBS and R-FIBS. All of the measurements reveal a higher ratio for the no. 3 pencil than the numbers 2.5 or 2, suggesting that the graphite concentration is highest in the no. 3 pencil. This is not anticipated as the no. 3 pencil is the hardest and thus has the least graphite concentration. In parts a and c of Figure 4 fs-LIBS, the no. 2 pencil has a slightly larger ratio than the no. 2.5. In parts b and d of Figure 4 R-FIBS, the numbers 2 and 2.5 are nearly the same ratio. The nonlinear and nonintuitive measurement for the carbon to aluminum ratio as a function of pencil hardness is attributed either to changes in the clay composition between pencil types or nonlinear changes in the graphite composition.

The graphite concentration was determined to be 37.7%, 39.0%, and 41.3% for numbers 3, 2.5, and 2, respectively, by optical microscopy. This strongly suggests that varying clay composition is responsible for the nonlinear concentration ratios displayed in Figure 4. Electron microprobe spectroscopy was used to independently measure the atomic constituents of the clay composition. The spectrum acquired for a no. 3 pencil can be seen in the Supporting Information. The spectrum contains K α lines from carbon (0.27 keV), oxygen (0.50 keV), magnesium (1.25 keV), aluminum (1.48 keV), silicon (1.73 keV), sulfur (2.33 keV), potassium (3.31 keV), calcium (3.69 keV), titanium (4.56 keV), and iron (6.45 keV). Sulfur, titanium, and calcium are known contaminants of the clay and will not be used in this analysis. Typical clays used in the Ticonderoga pencils are Illite (K_{0.6}(H₃O)_{0.4}Al_{1.3}Mg_{0.3}Fe_{0.1}Si_{3.5}O₁₀(OH)₂(H₂O)) and Kaolinite (Al₂Si₂O₅(OH)₄). The measured aluminum to silicon ratio

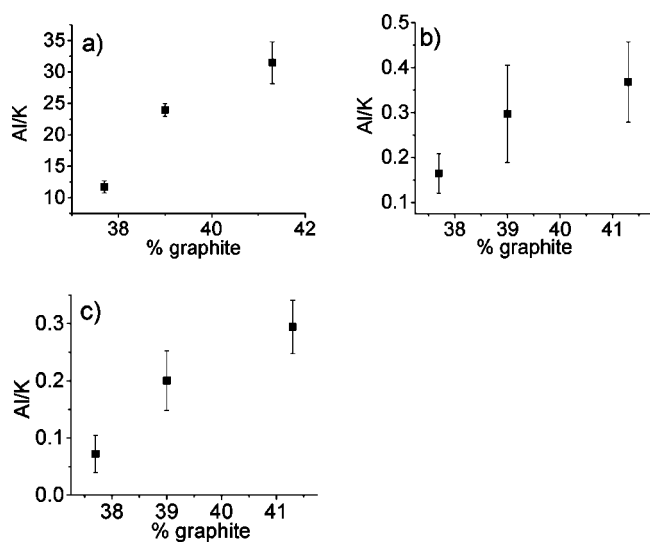
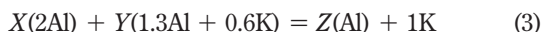


Figure 5. (a) Electron microprobe, (b) fs-LIBS, and (c) R-FIBS measurement of the Al/K emission line intensity ratio as a function of percent graphite in the composite.

changed from pencil numbers 2, 2.5, and 3, suggesting that the clay composition is not the same for each pencil. This is also shown in Figure 5a where the electron microprobe measurement of the aluminum to potassium ratio is shown for each sample. Illite contains potassium and thus the Al/K ratio can be used to determine the Illite to Kaolinite ratio in each sample. The no. 3 pencil, for example, has greater Illite concentration, as indicated by the lower Al/K ratio. Figure 5b,c shows the same Al/K trend for fs-LIBS and R-FIBS revealing that these methods have the potential for quantitative analysis.

With confirmation that the clay composition is changing as a function of pencil hardness, a straightforward comparison of atomic ratios (C_2/Al) cannot be used for discrimination between pencil types without correcting for the clay composition. The measurement of the C/Al ratio using the electron microprobe, shown in Figure 6a, reveals the same relative concentration ratio as the fs-LIBS and R-FIBS C_2/Al measurement shown in Figure 4. The electron microprobe data can be calibrated for the sample's matrix effects using the ZAF correction scheme (atomic number (Z), absorption (A), and fluorescence (F)) to obtain the absolute atomic concentrations in the clay. The atomic concentrations reveal the ratio of Kaolin to Illite clay via the stoichiometric formulas for each clay. We assumed the amount of potassium present in the composite was an indicator of the Illite concentration. Equation 3 shows the stoichiometric equation used to determine the ratio of Kaolin to Illite clay.



where Z is the Al/K atomic concentration ratio from the electron microprobe data, Y was the amount of Illite clay necessary (1.666) to balance the potassium terms of eq 3, and X was the amount of Kaolin clay in the mixture. The calculated Kaolin/Illite ratios were used to normalize the clay composition for each pencil from the microprobe data and the corrected plot of C/Al is shown in Figure 6b. A linear positive slope is obtained as would be expected if the clay composition was the same for the various pencil types. The same calculation can be performed to normalize the clay for the fs-LIBS and R-FIBS

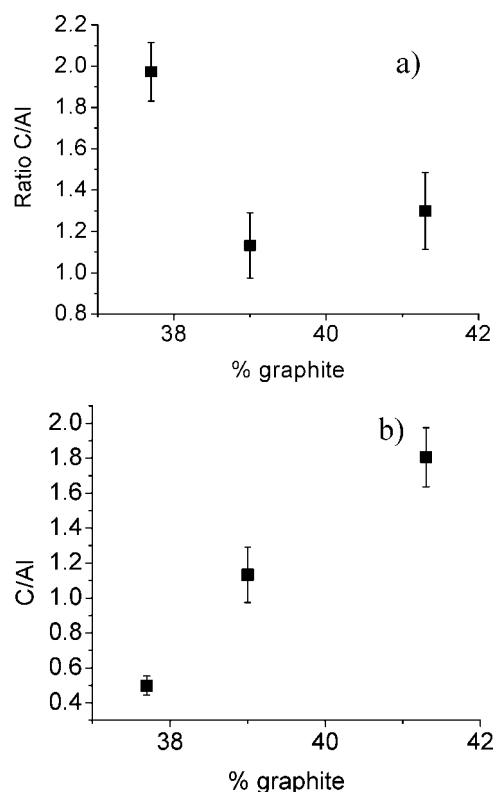


Figure 6. (a) Electron microprobe data for the C/Al ratio as a function of percent graphite in the composite. (b) Microprobe data for the C/Al ratio with the clay composition normalized.

data, but first the plasma temperature must be determined before the Kaolin/Illite ratio can be calculated for the laser-based analysis.

For this composite sample, the temperature can be calculated either from the C_2 Swan line intensities or from atomic emission intensities. The carbon lines presumably arise from the graphite regions and the metallic from the clay domains. Each estimate of the temperature (vibrational or electronic) relies on the Boltzmann distribution of population as a function of excited-state energy for a particular atom or molecule. For the electronic emission, we calculate the integrated line intensity equation, I_{ij} for the transition between upper level i and lower level j ,

$$I_{ij} = \frac{A_{ij} g_i}{U^s(T)} n^s e^{-E_i/kT} \quad (4)$$

where A_{ij} is the transition probability, g_i is the statistical weight of the upper level, $U^s(T)$ is the internal partition function of the species Al or K, n^s is the total number density of the species in the plasma, E_i is the excitation energy of the level, k is the Boltzmann constant, and T is the temperature, the n^s for aluminum and potassium can be calculated. The temperature was calculated via eq 4 using the intensity of the K I and Al I emission lines as measured by fs-LIBS and R-FIBS. The lines from these atoms were not used because multiple lines from any single atom (with energy spacing far enough apart to make an accurate calculation) were not detectable with our system. The ratio of number density for these atoms was assumed to be equal to the ratio measured by the electron microprobe. The temperature was

Table 1. Calculated Plasma Temperatures

	metallic ratio $n_{\text{Al}}/n_{\text{K}}$	C ₂ Swan
	fs-LIBS Plasma Temperature	
no. 2	9110 ± 800	5460 ± 1340
no. 2.5	7830 ± 600	5220 ± 1150
no. 3	8580 ± 600	5140 ± 850
	R-FIBS Plasma Temperature	
no. 2	10190 ± 450	4125 ± 190
no. 2.5	8970 ± 400	3870 ± 175
no. 3	8450 ± 300	3930 ± 490

then determined by solving eq 4 for temperature given the ratio of emission line intensities, number densities, and partition functions. The plasma temperature was also calculated for graphite using Boltzmann plots of the C₂ Swan system in our pencil spectra:

$$\log \sum_{v''} \frac{I^{v''}}{\lambda^4} = C_1 - \frac{G'(v')hc}{kT} \quad (5)$$

where I is line intensity, λ is the emission wavelength, h is Planck's constant, c is the speed of light, k is Boltzmann's constant, and $G'(v')$ are the term values of the vibrational states in the upper electronic level which is equal to

$$G = \omega_e \left(v + \frac{1}{2} \right) - \omega_e x_e \left(v + \frac{1}{2} \right)^2 + \omega_e y_e \left(v + \frac{1}{2} \right)^3 + \dots \quad (6)$$

Calculating Boltzmann ratios for the C₂ Swan System emission peaks, we were able to determine plasma temperatures but with large error bars. Table 1 displays the calculated plasma temperatures using the metallic emission ratio and Boltzmann plots of the C₂ Swan system emission. The C₂ Swan system temperatures were consistently lower than the clay atomic emission analysis temperatures. The difference in calculated plasma temperatures from C₂ emission bands and the clay atomic emission analysis may be attributed to nonequilibrium plasmas formed by microdomains of clay and graphite. The difference may also be due to different equilibrium temperatures for the

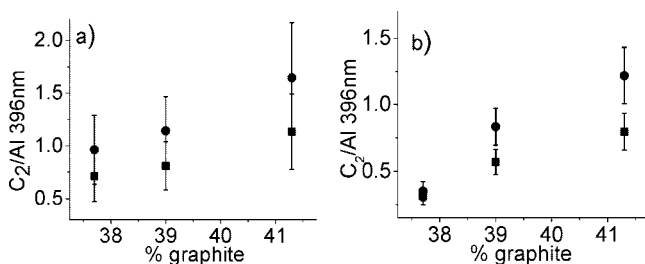


Figure 7. (a,b) Normalized C₂/Al ratios calculated using the temperature from laser-induced atomic emission lines (●) and with the temperature determined from the C₂ Swan system emission (■) for (a) fs-LIBS and (b) R-FIBS.

electronic and vibrational modes. Figure 7a,b shows the corrected clay plots of C₂/Al for fs-LIBS and R-FIBS. In the case of fs-LIBS, the error in the measurements is too large to make an accurate discrimination. In the case of R-FIBS, discrimination between pencil types is possible when the clay composition is determined.

In each of the measurements shown in Figures 4, 5, and 7, the FIBS data has smaller error bars. This is attributed to the intensity clamping property of laser filamentation described in the introduction. The self-governing nature of the laser intensity in the filament leads to a more stable plasma generation and, thus, a more constant signal intensity.¹⁹ The fs-LIBS measurement is more affected by laser fluctuations since the intensity is not regulated after the laser, resulting in larger shot to shot variation in signal intensity.

CONCLUSION

In this paper we investigated the fs-LIBS and R-FIBS analysis of a series of carbon targets mixed with varying degrees of clay materials. In the fs-LIBS experiment, a geometrically focused beam propagating through air was used to create a plasma from a carbon composite sample and the emission spectra was collected 10 m away with a telescope, spectrometer, and ICCD camera. In the R-FIBS experiment, a filament propagating through air was used to create a plasma on the sample. A comparable emission spectrum for each target was achieved using either plasma generation method. R-FIBS achieved better signal-to-noise than fs-LIBS due to intensity clamping of the filament, which produces a more stable ablation source. Discrimination between pencils was achieved once the clay composition was normalized. The calculated temperatures for the graphite of ~4500 K was lower than that calculated for the clay domain, ~8500 K.

ACKNOWLEDGMENT

This work was supported by the Army Research Office through Award No. 311390131, and the National Science Foundation. We acknowledge Dmitri Romanov for discussions regarding the effect of Kerr lensing on the focal spot size. We also acknowledge Jim Ladd and John Friel for discussions regarding electron microprobe analysis and Dennis Terry for assistance with the optical microscope analysis.

SUPPORTING INFORMATION AVAILABLE

Additional information as noted in text. This material is available free of charge via the Internet at <http://pubs.acs.org>.

Received for review October 2, 2008. Accepted February 4, 2009.

AC802080Q